Oxygen Permeation and Stability Study of (La0.6Ca0.4)0.98(Co0.8Fe0.2)O3- Membranes

Alternative title; Oxygen permeation and stability study of (La0.6Ca0.4)(0.98)(Co0.8Fe0.2)O3-delta membranes

Salehi, Mehdi; Søgaard, Martin; Esposito, Vincenzo; Foghmoes, Søren Preben Vagn; Persoon, E. S.; Schroeder, M.; Hendriksen, Peter Vang

Published in:
Journal of Membrane Science

Link to article, DOI:
10.1016/j.memsci.2017.07.050

Publication date:
2017

Document Version
Peer reviewed version

Oxygen Permeation and Stability Study of $(La_{0.6}Ca_{0.4})_{0.98}(Co_{0.8}Fe_{0.2})O_{3-\delta}$ Membranes

M. Salehi, M. Søgaard, V. Esposito, S.P.V. Foghmoes, E.S. Persoon, M. Schroeder, P.V. Hendriksen

www.elsevier.com/locate/memsci

PII: S0376-7388(17)31049-9
DOI: http://dx.doi.org/10.1016/j.memsci.2017.07.050
Reference: MEMSCI15455

To appear in: *Journal of Membrane Science*

Received date: 12 April 2017
Revised date: 9 July 2017
Accepted date: 27 July 2017

Cite this article as: M. Salehi, M. Søgaard, V. Esposito, S.P.V. Foghmoes, E.S. Persoon, M. Schroeder and P.V. Hendriksen, Oxygen Permeation and Stability Study of $(La_{0.6}Ca_{0.4})_{0.98}(Co_{0.8}Fe_{0.2})O_{3-\delta}$ Membranes, *Journal of Membran Science,* http://dx.doi.org/10.1016/j.memsci.2017.07.050

Oxygen Permeation and Stability Study of $(La_{0.6}Ca_{0.4})_{0.98}(Co_{0.8}Fe_{0.2})O_{3-\delta}$ Membranes

M. Salehi[1,2*], M. Søgaard[1,3], V. Esposito[1], S.P.V. Foghmoes[1], E.S. Persoon[4], M. Schroeder[4] and P.V. Hendriksen[1*]

[1]Department of Energy Conversion and Storage, Technical University of Denmark, Frederiksborgvej 399, 4000 Roskilde, Denmark

[2] Current address: The Federal Institute for Materials Research and Testing (BAM), Unter den Eichen 44-46, 12203 Berlin, Germany

[3] Current address: Meneta Danmark ApS & Meneta Advanced Shims Technology A/S Kirkegyden 52, DK-5270 Odense N, Denmark

[4] Institute of Physical Chemistry, RWTH Aachen University, Landoltweg 2, D-52056 Aachen, Germany

*Corresponding authors:

M. Salehi, E-mail address: chemehdi3333@gmail.com

P.V. Hendriksen, E-mail address: pvhe@dtu.dk

Abstract

The perovskite-type oxide $(La_{0.6}Ca_{0.4})_{0.98}(Co_{0.8}Fe_{0.2})O_{3-\delta}$ (LCCF) was investigated for use as oxygen separation membrane. A 25µm thick dense membrane on a porous LCCF support with a thickness of around 175 µm was prepared by a tape casting and lamination process. The optimum sintering temperature of the component was established to be 1050°C by analysis of microstructures of membranes sintered at different temperatures. Scanning electron microscopy (SEM) examination of cross-sections of the sintered membrane showed that it consisted of two phases, the main phase being enriched in calcium (Ca) and depleted in lanthanum (La), relative to the nominal

composition. A surface activation layer of LCCF was deposited onto the dense layer to increase the exchange rate of oxygen at the surface. For the coated membrane, the oxygen permeation flux increased with temperature and reached a maximum value of 3.32 Nml cm^{-2} min^{-1} at 900°C when, for characterization purpose pure oxygen was used as feed and a maximum value of 2.06 Nml cm^{-2} min^{-1} at 900°C was obtained when air was used at the feed side, both with N_2 sweep on the permeate side. The stability of the membrane against sulfur dioxide (SO_2) and pure carbon dioxide (CO_2) was tested. A small decrease in the flux was observed over 48 h in CO_2 at 850°C. SEM examinations of the cross-section of the tested membrane showed that the Ca rich phase in the membrane showed a tendency to migrate to the feed side. **Whereas the material shows a CO_2 stability superior to that of Sr or Ba containing analogues, the material stability is not sufficient for applications requiring direct exposure to sulfur-rich flue gases.**

Keywords: oxygen permeation membrane, kinetic demixing, stability, oxy-fuel

1. Introduction

Global climate change induced by the anthropogenic emission of greenhouse gases such as carbon dioxide (CO_2) is of great concern as it can lead to serious climate changes [1]. The largest emitter of CO_2 emissions is the energy sector and reduction and/or sequestration of CO_2 emitted from fossil fuel power plants is therefore receiving attention in many countries [1, 2]. Oxy-fuel combustion is a promising process for facilitating the separation of CO_2 from the exhaust gas mixture, with a view to reuse of CO_2 for enhanced oil recovery or for sequestration [3, 4]. The fuel is combusted with pure oxygen mixed with flue gas and the final reaction products are steam and CO_2 only (It may contain other elements in small amounts due to impurities in the fuel feedstock and leaks).

From such a mixture, the capture and sequestration of CO_2 can be carried out with a smaller energy penalty than amine-based CO_2 separation process [2, 5].

Cryogenic distillation is usually used industrially for large scale production of oxygen. This process is quite energy intensive and requires 200-400 kWh/ton O_2, depending on the size of the plant [5, 6]. A significant effort is therefore devoted to research on the development of more energy efficient oxygen separation techniques [7, 8]. Oxygen Transport Membranes (OTMs) are among the alternative technologies that could replace the traditional process for oxygen production in industry. A clearly noticeable reduction of the energy associated with the oxygen production is likely achievable if the OTMs are integrated with the combustion process [3, 5, 9, 10] . An OTM consists of a gastight mixed ionic /electronic conducting (MIEC) material that allows diffusion of oxygen ions via vacancies in the crystal lattice and a counter-balancing electronic transport. The driving force for the oxygen ion transport is established by a difference in the partial pressure of oxygen between the two sides of the membrane [6].

Many complex oxides have been synthesized and investigated for the use of OTMs, and some of the most frequently considered MIEC materials are perovskite compounds belonging to the broad classes of $(Ba,Sr)(Co,Fe)O_{3-\delta}$ and $(La,Sr)(Co,Fe)O_{3-\delta}$ [11]. However, these materials have drawbacks including: i) chemical instability at low oxygen partial pressures, ii) reactions with gas-phase components like SO_2 and CO_2 even when these are present in small concentration (a few hundred ppm), and iii) the materials may undergo a degradation process known as kinetic demixing, where the multicomponent material becomes chemically inhomogeneous. To address these problems, intensive efforts have been made to develop OTMs that combine high oxygen flux with long term stability at high operating temperature [3, 11, 12]. Replacing Sr with Ca, $(La_{0.6}Ca_{0.4})(Co_{0.8}Fe_{0.2})O_{3-\delta}$ (LCCF) is expected to make the material less prone to reaction with CO_2 as $CaCO_3$ is less stable than $SrCO_3$ [13, 14].

Teraoka *et al.* first reported a very high oxygen permeation flux, about 1.8 cm^3 (STP) cm^{-2} min^{-1} at around 870ºC in an air/He gradient, for a $(La_{0.6}Ca_{0.4})(Co_{0.8}Fe_{0.2})O_{3-\delta}$ membrane (ca. 1.5 mm thick) in the late 1980s [15]. Also, a maximum oxygen permeability of 4.8 cm^3 (STP) cm^{-2} min^{-1} at 930ºC in an air/He gradient was obtained for a $(La_{0.6}Ca_{0.4})(Co)O_{3-\delta}$ (LCC) dense supported asymmetric structure (dense layer ≈ 10μm) coated with a porous LCC catalyst layer [16]. Later a lower value of 1.66 cm^3 (STP) cm^{-2} min^{-1}, for the same asymmetric-structured system without activation layer was reported [17]. Stevenson *et al.* reported the oxygen permeation flux of around 0.07 cm^3 (STP) cm^{-2} $min^{-1}$and 0.03 cm^3 (STP) cm^{-2} min^{-1} at 900ºC in O_2 [pO_2=1atm]/ N_2 gradient, respectively, for a $La_{0.4}Ca_{0.6}Co_{0.2}Fe_{0.8}O_{3-\delta}$ and a $La_{0.4}Ca_{0.6}Co_{0.8}Fe_{0.2}O_{3-\delta}$ dense membranes with thickness of 2-3 mm [18]. They also observed some additional phases such as $Ca_2Fe_2O_5$, $Ca_2Co_2O_5$, $CaFe_2O_5$, and CoO after calcination of powders in air at 850°C and sintering of membranes in air at 1200°C [18]. Diethelm *et al.* investigated disc-shaped $La_{0.4}Ca_{0.6}Fe_{1-x}Co_xO_{3-\delta}$ (x=0, 0.25 and 0.5) membranes with different thicknesses (from 0.72 to 1.73 mm) [19]. The largest flux was found for the membranes with the highest content of Co in an air/argon gradient at 800-900°C (around 0.09 cm^3 $cm^{-2}min^{-1}$ at 900°C for a $La_{0.4}Ca_{0.6}Fe_{0.5}Co_{0.5}O_{3-\delta}$ membrane with a thickness of 1.4 mm). More recently, Efimov *et al.* investigated the chemical stability and oxygen ionic conducting properties of compositions in the $(La_{1-x}Ca_x)(Co_{0.8}Fe_{0.2})O_{3-\delta}$ (x=0.4–0.6) system [13]. It was found that the component with the lowest amount of Ca (x=0.4) was almost a pure perovskite phase while the materials with more Ca included a significant content of secondary phases after calcination at 900°C. *In situ* XRD measurements showed a good stability of LCCF materials against CO_2. A flux of 0.66 cm^3 cm^{-2} min^{-1} in an air/ He gradient was reported at around 950°C for an asymmetric LCCF membrane with a dense layer of thickness of about 10μm. The LCCF membrane showed a high stability in CO_2, with a constant oxygen permeation flux being observed over

200 h. They observed a non-perovskite phase in the tested membrane ($La_{0.6}Ca_{0.4}Co_{0.8}Fe_{0.2}O_{3-\delta}$), and proposed that the foreign phases originated already from the synthesis of the LCCF powder and sintering of the membrane [13].

Despite the high oxygen permeability and a good tolerance against CO_2, little is known about the membrane stability in SO_2 containing atmosphere and about the rate of a possible kinetic demixing at high temperatures. The kinetic demixing due to long term exposure to a chemical gradient may lead to generation of new secondary phases and affect the performance of the membrane. Therefore, in this work a detailed study elucidating the stability of the LCCF membrane against SO_2 and pure CO_2 with focus on the kinetic demixing and stability has been conducted.

2. Experimental

2.1 Sample preparation

The support and membrane layer were both manufactured by tape casting using slurries based on $(La_{0.6}Ca_{0.4})_{0.98}(Co_{0.8}Fe_{0.2})O_{3-\delta}$ (Topsoe Fuel Cells, Denmark) powder with a specific surface area of 2.2 m^2 g^{-1} after calcination for 6 h at 900°C. **The powder was synthesized via a drip pyrolysis method at low temperature of about 550°C [20].** A graphite powder (V-UF1 99.9% purity, Graphit Kropfmühl Germany) was used as pore former for the porous support tapes. Tape casting slurries were prepared by dispersing the LCCF powder in ethanol using polyvinylpyrrolidone (PVP). The mixtures were typically ball milled for 72 h in PE bottles using zirconia balls. After milling, the median particle size (d_{50}) was typically around 1.0 µm. A PVB based binder system is then added and the slurries were rotated further for another 24 h to allow a proper homogenization. For the porous layer, graphite powder was further added. The slurries were finally filtered, using a 40 µm sieve, and de-aired at a vacuum of around 0.3 bar before tape casting onto a polymer film. The

porous layer was tape-cast at a height of 1.25 mm, and the dense layer at 200 μm using a double doctor blade system and a casting speed of 20-30 cm min^{-1}. Green tapes were then dried at room temperature for several days and then co-laminated using a lamination machine (Fujipla, Japan) at 160 °C at a speed of 0.4 m min^{-1}. The green tapes were punched into disk shaped samples and subjected to thermal debinding to remove the binders at a very slow heating rate (15°C h^{-1}), and subsequently sintered in air at 1050°C for 3 h (the heating rate was 20°C h^{-1}). This resulted in a dense thin membrane ≈ 25 μm supported on porous LCCF support ≈175 μm. A porous LCCF layer was subsequently deposited on the dense side of the membrane. An ethanol based slurry of LCCF for spray coating was prepared from the calcined LCCF powder. After coating, the samples were fired at 900 °C for 2 h.

2.2 Basic characterization of powders and membranes

Phase analysis of the calcined powders and membranes was performed by X-ray diffractometry (XRD) in the 2Θ range from 15 to 90º in a Bruker AXS D8 Discover diffractometer operated at 40 kV and 40 mA, with Cu Kα radiation (1.54056 Å). Thermogravimetry (TGA) (Netzsch STA 409CD) was carried out from room temperature to 900°C with a heating rate of 10°C min^{-1}. The LCCF powder was placed in an open Pt crucible. All TGA was carried out in air or in pure CO_2 (oxygen content approximately 10^{-5} atm) with a flow rate of 50 cm^3 min^{-1}.

The gas tightness of the membranes was verified by an in-house constructed leak tester (leak rates less than 0.1 ml min^{-1}) at room temperature. Scanning electron microscopy (SEM) (Hitachi TM-3000, Japan) combined with energy dispersive spectroscopy (EDS) was used to characterize the microstructure of the membranes (prior to and after testing). A Carl Zeiss SUPRA 35 FEG-SEM was used for high resolution imaging. Elemental analysis was carried out using EDS with a Thermo Electron Corporation detector. A stability test of the

membrane material towards sulfur dioxide was performed. The material was exposed to a gas containing 400 ppm of SO_2 at 850°C over 48 h. The setup is illustrated in Figure S1 in the supporting material. After the exposure, samples were analyzed by means of XRD, SEM and EDS.

2.3 Permeation measurements

The set-up used for oxygen permeation experiments is shown in **Figure S2 in Supporting materials**. Measurements and data analysis (oxygen permeation and estimation of gas leakages) were carried out as has been described previously [21, 22]. The membrane was placed between two alumina tubes with an inner diameter of 8.7 mm. **The porous LCCF support and the LCCF membrane were, respectively, at the feed side and at the permeate side.** A seal based on an in-house developed glass paste (prepared from sodium aluminosilicate (NAS) powder and organic additives [22, 23]) was applied at the tube/membrane interface to ensure gas-tightness. The tests were performed in a temperature range from 800 to 900°C at various oxygen partial pressures (pO_2) at each temperature. Air (pO_2=0.21) or pure oxygen (pO_2=1) was used on the feed side, while a mixture of N_2 or CO_2 was used as sweep gas on the permeate side. Oxygen was separated from air by solid state ambipolar diffusion through the dense membrane due to the oxygen partial pressure gradient and released on the permeate side. The gas flows were controlled using calibrated mass flow controllers. The total permeate flow was measured using a mass flow meter. The oxygen partial pressure, pO_2, in the inlet gas, $p_{O_2}^{in}$, and outlet gas, $p_{O_2}^{out}$, streams were monitored using an in-house build oxygen sensor. The oxygen permeation flux was calculated from the mass balance:

$$j_{O_2} = \frac{V_{in}(P_{O2}^{out} - P_{O2}^{in})}{P_{tot}A} \qquad (1)$$

where j_{O_2} is the oxygen permeation flux through the membrane (Nml $cm^{-2}min^{-1}$), V_{in} is the effluent carrier gas flow (Nml min^{-1}) and *A* is the effective membrane surface area (cm^2).

3. Results and discussion

3.1 Characterization of powders and membranes

XRD analysis revealed a cubic perovskite structure (with the detection of minor impurity phases **such as La_2O_3**, see the inset in Figure 3) after calcination of the LCCF powder at 900°C for 6h. The lattice parameter was 3.8226Å (space group Pm-3m) determined by the Rietveld refinement, in agreement with literature data [13, 18].

Figure 1 shows the TGA data (relative mass changes) of the non-calcined LCCF powder in air and pure CO_2 with consecutive heating/cooling cycles. The LCCF powder was first heated up to 900 °C and cooled down in air, then the atmosphere was switched to pure CO_2 and the sample was re-heated to 900 °C and back to 50°C. Finally, the sample was heated up and cooled down in air. The TGA results are summarized in Table 1.

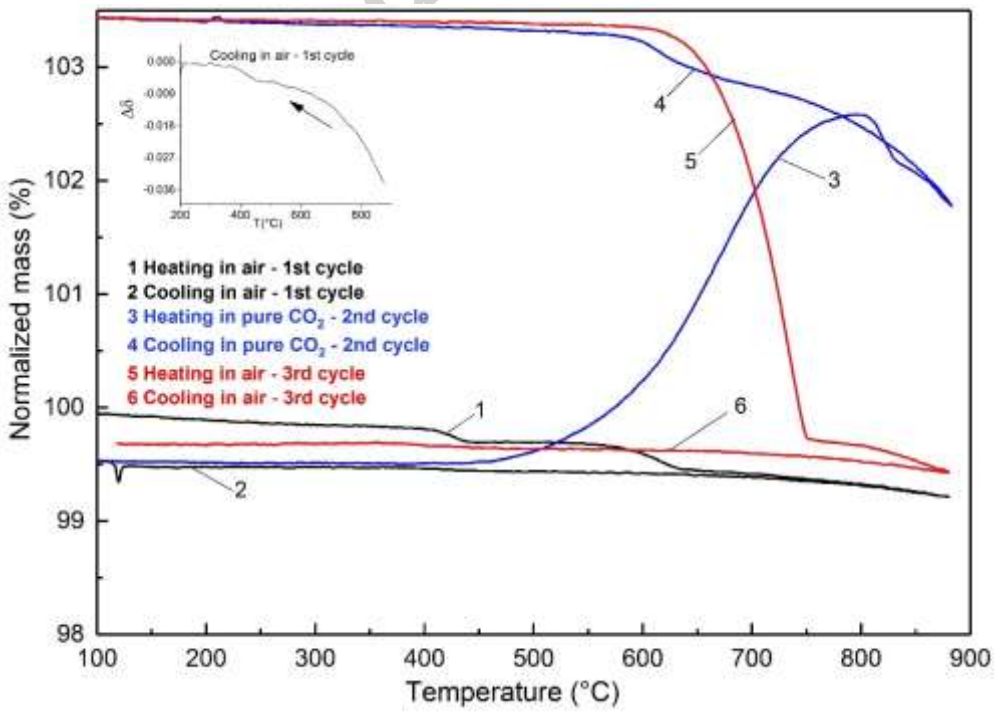

Figure 1. Normalized mass change as a function of temperature of the LCCF powder in air and CO_2.

Table 1. Mass loss and mass gain in percentage during heating and cooling of the LCCF powder in air and CO_2 atmospheres.

Heating/Cooling cycle	Heating	Cooling	Atmosphere
1st (steps 1 and 2)	-0.79%	+0.33%	Air
2nd (steps 3 and 4)	+2.33%	+1.67%	CO_2
3rd (steps 5 and 6)	-4.01%	+0.25%	Air

As can be seen from Table 1, the powder lost 0.79% weight and regained 0.33%, during heating and cooling, respectively, in the first cycle. The mass losses corresponding to the two steps at about 420°C and 620°C are probably caused by the presence of impurities such as carbonate groups in the raw powder. The mass loss and gain during heating and cooling above 650°C in air corresponds to the change in oxygen stoichiometry of the perovskite [24]. The inset in Figure 1 shows the calculated oxygen non-stoichiometry in air of the LCCF based on the cooling curve (step 2). In a pure CO_2 atmosphere (oxygen content approximately 10^{-5} atm), the sample showed a mass gain of approximately 2.33% during heating and 1.67% during cooling. This is most likely due to carbonate formation [25, 26]. Heating up again in air (step 5) the sample exhibited a mass loss of 4.01%, which equals the sum of the mass gains in the steps 3 and 4. The onset temperatures for carbonate formation and decarbonation in a CO_2 atmosphere are about 450ºC and 810ºC, respectively. Similar reversible mass gains and losses were previously reported for perovskite-type ($(Ba, Sr)(Co, Fe)O_{3-\delta}$ and $La_{0.6}Sr_{0.4}CoO_{3-\delta}$) oxides [25-27], but for the Ca containing material studied here the carbonate decomposes more readily than reported for the Sr and Ba rich compounds studied in [25, 26]. In this work, carbonate decomposition occurs at ~810 ºC, compared to 980 ºC found for the Sr-containing material [26]. For the Ba-containing material,

carbonate decomposition was also found around 800°C [25] but in a dilute CO_2 atmosphere unlike here, where measurements were carried out in pure CO_2. These differences reflect the lower stability of $CaCO_3$ **[28]** compared to $SrCO_3$ and $BaCO_3$. The material stability under high CO_2 activity is clearly superior to that of Ba and Sr containing analogues and does not seem a limiting factor for its use.

Several experiments were performed to determine the optimum sintering temperature for the membranes. After sintering at 1000°C, a large amount of porosities were observed in the membrane layer. On the other hand at 1100°C, the porosity in the porous support layer decreased and a rather dense structure developed (**see Figure S3 in Supporting materials**). Therefore, 1050°C was chosen as the sintering temperature for the component manufacture.

Figure 2 shows a typical SEM micrograph of the LCCF membrane sintered at the optimum temperature (=1050°C) with an activation layer composed of the same material on top of the dense layer. The coated layer is highly porous and is well attached on the dense layer with a homogeneous thickness of approximately 5µm. The support contains randomly distributed pores up to 8 µm with an overall porosity of about 35±3% (determined by image analysis) while the dense layer shows a very low closed porosity and no cracks. The gas tightness was confirmed **on the membrane layer** by an in-house constructed leak tester at room temperature. The samples showed a leak rate of approximately <0.1 ml min^{-1}, which is in the same range as a dense steel calibration sample.

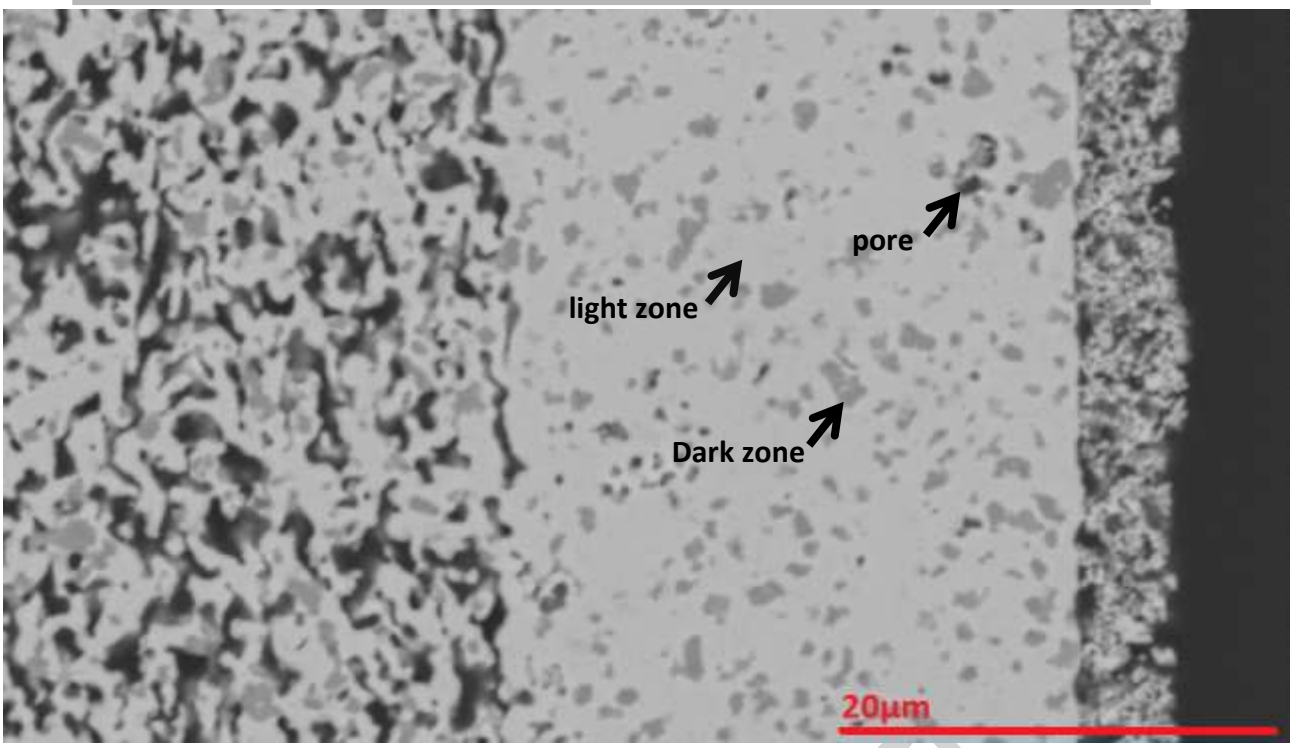

Figure 2. SEM micrograph from cross-section of the polished membranes sintered at 1050°C/3h.

Figure 2 also clearly shows that the membrane sintered at 1050°C consists of two phases. The atomic composition of the different phases has been determined using EDS. Results are listed in Table 2. The EDS elemental mapping (see Figure S4 in supporting materials) revealed that the secondary phase (dark phase) is enriched in Ca and depleted in La relative to the dominant phase whereas the Fe, Co and O content seems to be the same in two phases. The amount of the Ca-enriched phase estimated by image analysis is about 15±2%. The observation of two phase structure is well in agreement with previous studies that have indicated the solubility limit of Ca in $LaCoO_3$ is around 28% (the formation of secondary phases such as Co_3O_4, CaO and CoO has been reported for 30% and higher mol% Ca doping on the A site) [29].

Table 2. The summary of EDS analysis on the LCCF membrane sintered at 1050°C/3h in air.

Element* (at. %)	La L	Ca K	Co K	Fe K	O K	Calculated composition

Average **	13.30±1.3	10.70±0.98	22.30±0.25	3.23±0.20	50.50±1.6	$La_{0.54}Ca_{0.46}$ $Co_{0.87}Fe_{0.13}$ O_x
Light zone	15.62±0.30	8.20±0.20	22.30±0.10	3.28±0.20	49.97±0.40	$La_{0.65}Ca_{0.35}$ $Co_{0.86}Fe_{0.14}$ O_x
Dark zone	5.05±0.70	20.58±0.50	21.94±0.20	3.26±0.30	49.15±0.60	$La_{0.13}Ca_{0.87}$ $Co_{0.89}Fe_{0.11}$ O_x

*The values for each element are the average of quantitative analysis on four different areas of the samples.
** Average represents both light and dark zones.

Figure 3 displays the XRD pattern of the dense layer of the membrane, showing some additional peaks corresponding to several secondary phases, the main one has different peaks close to those from $Ca_2(Co, Fe)_2O_5$. It is worth noting that the main peaks of $Ca_2(Co, Fe)_2O_5$ structure are indexed in the same position as those of perovskite structure.

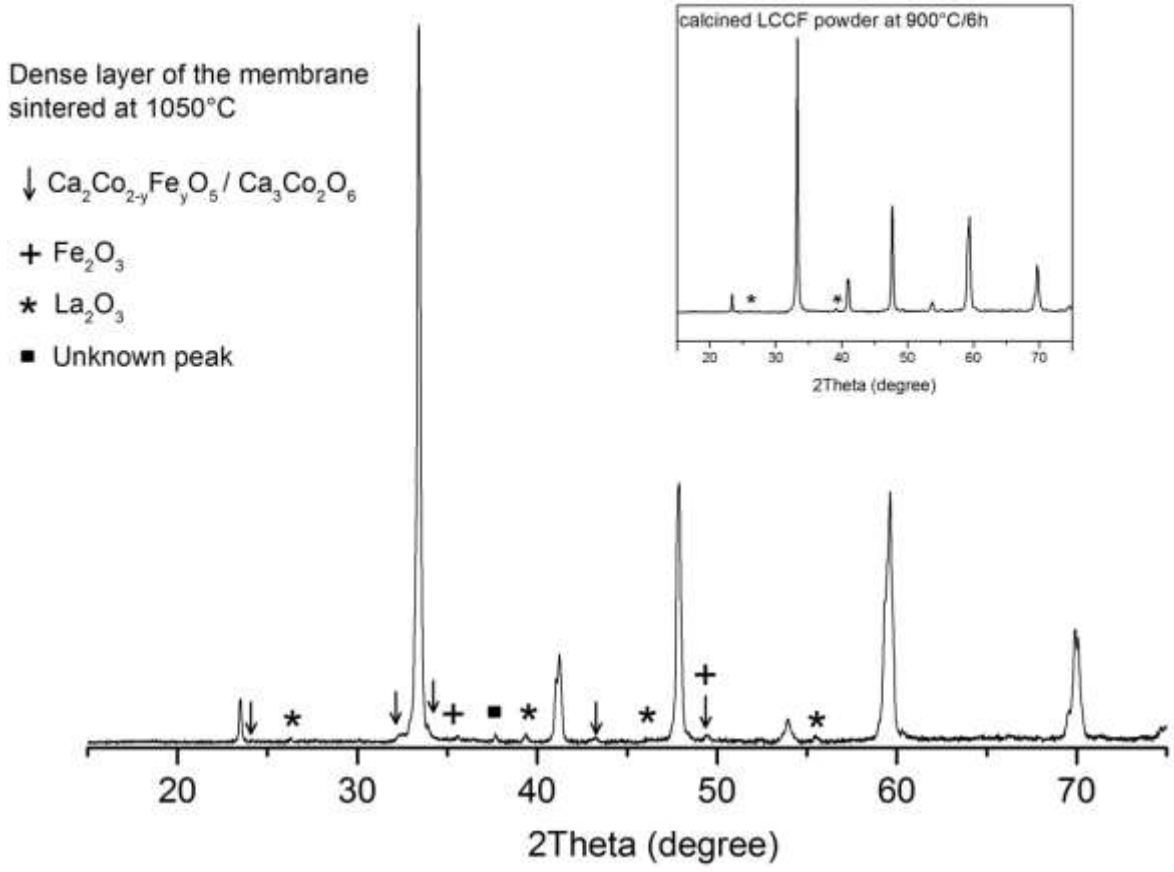

Figure 3. XRD pattern of dense layer of the membrane sintered at 1050°C/3h (The inset shows the XRD patterns of the calcined LCCF powder).

3.2 Oxygen permeation test

Figure 4 shows the oxygen permeation fluxes through an uncoated and a coated membrane **versus overall apparent driving force (log (pO_2''/pO_2'))** for

different temperatures and feed gas compositions. Note that in Figure 4a the feed stream is air and in Figure 4b the feed stream is pure oxygen. **The reader is reminded here that the porous support layer was placed on the feed side in this study.**

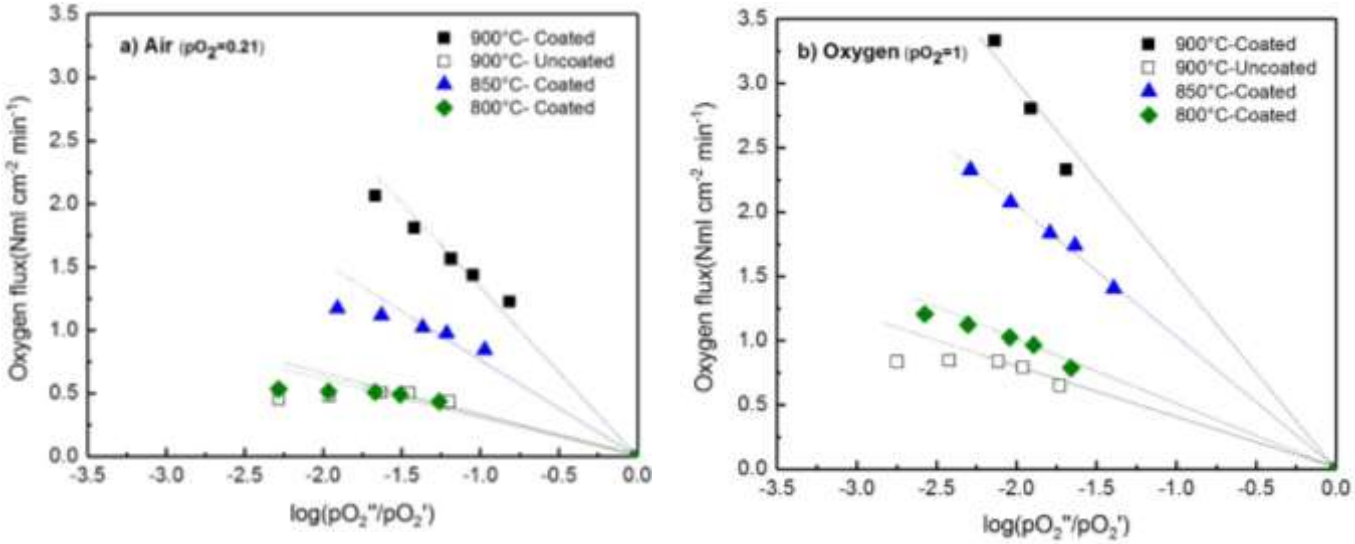

Figure 4. Oxygen permeation rate through the uncoated and coated membranes as a logarithmic function of oxygen partial pressure: a) feed= air and b) feed= pure oxygen.

At 800 – 850°C the fluxes were very small for the uncoated membrane and due to the high experimental uncertainty in their determination the measurements are not reported here. The pO_2 on the permeate side was adjusted by varying the N_2 flow rate from 16.7 to 200 ml min^{-1}. As the oxygen content of the inlet gas in all cases was below 10^{-5} atm the variations on the outlet oxygen partial pressure are caused by the oxygen permeating the membrane. The oxygen flux at 900°C for the coated membrane was: 2.06 Nml cm^{-2} min^{-1} and 3.32 Nml cm^{-2} min^{-1} for the case of air and oxygen on the feed side, respectively. Modification of the membrane surface strongly improved the oxygen permeation, which is well in line with numerous earlier studies on other types of membranes [30-34] where the oxygen permeation is jointly controlled by bulk diffusion and surface exchange reactions or only governed by surface exchange reactions [30, 32]. The enhancement of the oxygen permeation flux by coating such a porous layer is related to the increase in the area over which the exchange process can take

place [30, 35]. **With pure oxygen as feed, the flux through the membrane clearly scales in direct proportion to the overall driving force. Some deviation from this trend is observed in the case of air on the feed side, where the measured fluxes at the lowest pO_2s fall below the linear trend curve. This indicates that mass transfer in the porous supports starts affecting the flux; some of the "driving force" is lost over the support. This reduces the flux directly, but also indirectly via its effect on the pO_2 at the surface of the membrane, which is reduced, leading to slower oxygen incorporation as $k_{surface}$ decreases with decreasing pO_2.**

Table 3 lists the apparent activation energy (E_a) values calculated for the coated membrane at a fixed log (pO_2''/pO_2') from Arrhenius plot of $\ln j_{O2}$ vs. 1/T (K) for different feed compositions. From literature on the perovskite-type membranes the activation energies of oxygen ion diffusion via the bulk and the oxygen surface exchange on the surfaces of the membrane are typically different, the latter being the higher [10, 36]. The values dependent on the membrane material and measurement conditions. For instance, Stevenson *et al.* reported activation energies of about 173 kJ mol^{-1} and 67 kJ mol^{-1} for the oxygen ion conduction of the $La_{0.4}Ca_{0.6}Co_{0.8}Fe_{0.2}O_{3-\delta}$ and $La_{0.4}Ca_{0.6}Co_{0.2}Fe_{0.8}O_{3-\delta}$ membranes (thickness =2-3 mm), respectively [18]. Li *et al.* reported a value of 144 kJ mol^{-1} for the oxygen permeation of a $La_{0.2}Ca_{0.8}Co_{0.2}Fe_{0.8}O_{3-\delta}$ dense membrane with the thickness of 1 mm [37]. **Here, apparent activation energies for the coated membrane of 153 ± 2 kJ mol^{-1} and 115 ± 2 kJ mol^{-1} (at a fixed pO_2 gradient) were obtained for the case of air and oxygen feed, respectively.**

Table 3. Apparent activation energies (*Ea*) determined for coated membrane at a fixed log (pO_2''/pO_2') **in the temperature range of 800-900°C.**

	Feed composition - Air ($pO_2 \approx 0.21$)	**Feed composition - Pure oxygen ($pO_2 \approx 1$)**
$\log(pO_2''/pO_2')$	Ea (kJ mol^{-1})	Ea (kJ mol^{-1})
-0.75	150	112
-1.00	154	113
-1.25	156	115
-1.50	-	116
-1.75	-	117
-2.00	-	119

The analysis of the activation energies determined for the oxygen fluxes is complicated since several different thermally activated processes play a role. The oxygen transport across a supported membrane occurs via sequential processes: 1) diffusion through the porous support, 2) incorporation in the material close to the dense layer, 3) diffusion through the bulk, and finally 4) re-oxidation and ex-corporation at the permeate side. Finite rate of the transport through the gas phase in the porous support may give rise to a concentration polarization. When gradients in the support are significant it leads to a reduced driving force for the bulk transport. The concentration polarization can be neglected for the pure oxygen case, but not for the measurements in air. Whereas, the oxygen in/ex-corporation and bulk diffusion are all thermally activated processes the concentration polarization is only mildly temperature dependent [38]. The determined values of *Ea* are thus not representative of one individual step only and are hence difficult to interpret unambiguously, however, the data presented in Figure 4 and Table 3 demonstrate an increased effect of the interfacial exchange resistances on the flux with reduced pO_2 both on high and low pO_2 side. With decreasing permeate side pressure the losses at the surface becomes larger leading to slightly stronger temperature dependence (*Ea* increases from 150 to 160 kJ/mol). Going from oxygen to air the losses at the

surface become relatively more important and the overall flux becomes smaller and more temperature dependent.

It can be also seen from Figure 4 that, for the uncoated membrane, the oxygen permeation at 900 °C does not continuously increase with an increasing oxygen partial pressure gradient across the membrane. Such a behavior has been reported previously for $La_{0.5}Sr_{0.5}Co_xFe_{1-x}O_{3-\delta}$ (x=0, 0.5, and 1) membranes [39] and for a $SrSc_{0.05}Co_{0.95}O_{3-\delta}$ membrane [40]. In those cases it has been associated with surface exchange kinetics that become fully rate-determining at low oxygen partial pressures. It is well known that the surface exchange kinetics become slower when the oxygen partial pressure is lowered [39, 41, 42]. In this case, the resistance associated with surface exchange simply increases more than the corresponding increase in driving force when lowering the oxygen partial pressure on the permeate side.

One could speculate that the effect originates from a decrease in temperature due to a higher flow on the permeate side, however, this can be ruled out as the coated samples should then show a similar tendency. In addition, the temperature during oxygen permeation tests was controlled with an uncertainty of less than 0.4%.

The short-term membrane stability was also studied at 850ºC using air on the feed side and pure CO_2 as sweep gas. Figure 5 shows the time dependence of the oxygen permeation flux for the LCCF membrane using pure CO_2 as sweep gas at 850ºC during approximately 48 h. A small decrease in the flux was observed within the testing period, corresponding to a decline of flux of 14% pr. 1000 h of extrapolated.

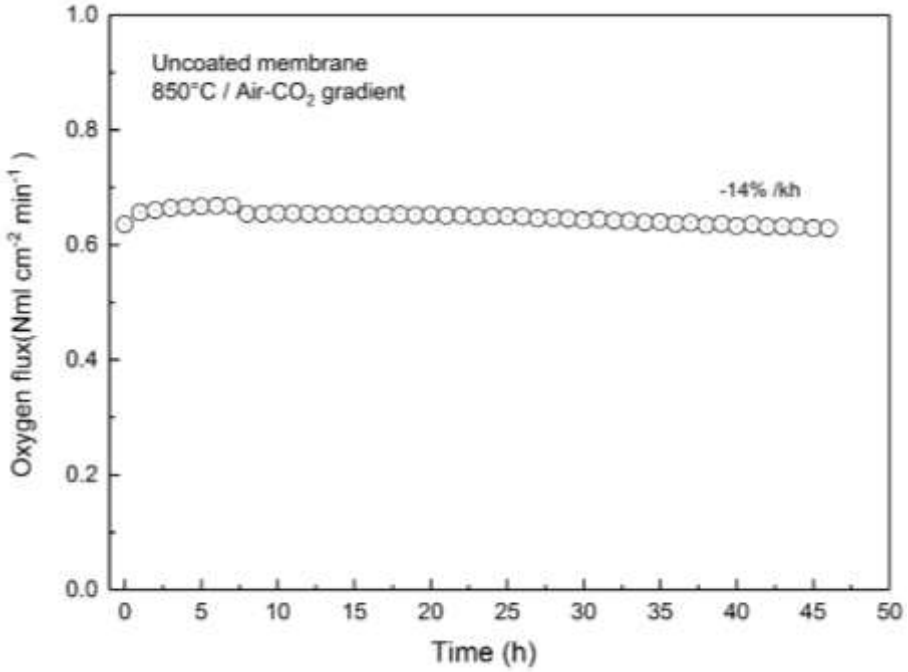

Figure 5. Oxygen permeation flux through the sintered supported LCCF membrane (thickness of membrane 25μm) as s function of time at 850ºC under air flow rate of 100 ml min^{-1} and CO_2 sweep gas of 200 ml min^{-1}.

3.3 Post-test examination

The membrane cracked during cooling of the permeation set up. The cracking of the membrane is attributed to the difference in the thermal expansion of the membrane and the contacting alumina tubes. The coefficient of thermal expansion of the LCCF was determined by *in-situ* XRD to be ca. 20×10^{-6} K^{-1} [13] and for alumina the CTE is around 8×10^{-6} K^{-1} [43]. On the feed side, the central part of the tested membrane, which was directly contacted by air, showed a change in color. However, there was no obvious change in color on the permeate side of the membrane.

XRD patterns of both sides of the membrane after oxygen permeation test were compared to those measured for the non-tested sample. The results are presented in Figure 6 and show that the perovskite structure remains intact at both surfaces of the membrane; however, some additional peaks were detected, which are related to the secondary phases formed, like $CaAl_2Si_2O_8$ (ICSD#654).

These phases are due to a reaction between the applied glass sealant materials and the membrane.

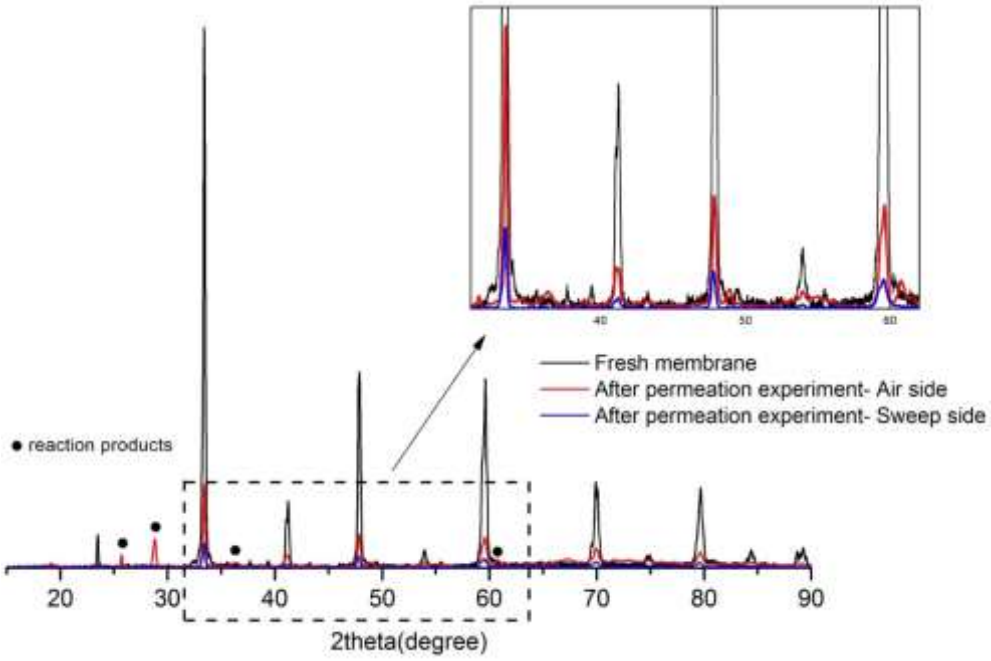

Figure 6. XRD patterns of the fresh membrane and both sides of the tested membrane.

Figure 7 shows a SEM image of a polished cross-section of the uncoated membrane after the permeation experiments **(see Figure S5 and Table S1 for details)**. A higher porosity has developed approximately up to 10 µm from the permeate side. In addition, a thin porous layer with a thickness of up to 1 µm is present on the surface of the permeate side. Further, the SEM-BSE image shows that a dark phase is abundant between the support layer and the membrane layer. The EDS analysis reveals that this phase is the Ca/Co rich phase (also discussed for the as-prepared membrane see Figure 2 and Figure S6 in supporting materials). The corresponding EDS line profiles of the cations across the uncoated and coated membranes are shown in Figure 8. **Similar behavior has been observed when the LCCF membrane tested under air/N_2 gradient at 850ºC for 36 h (Fig. S7 in Supporting materials).**

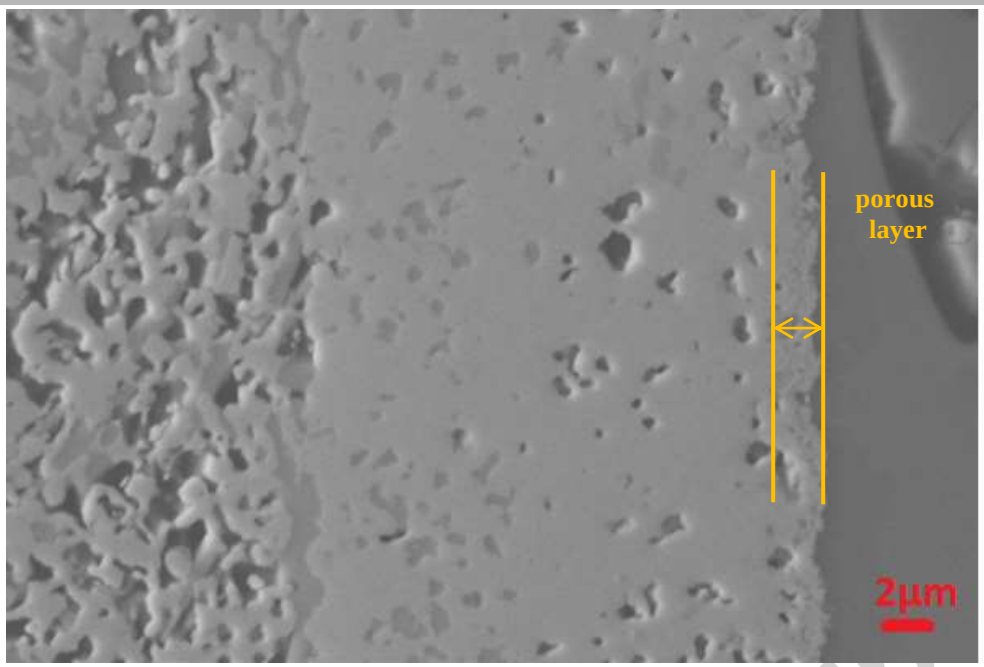

Figure 7. SEM-BSE image fracture of cross-section of the membrane after durability test. Air was applied on the support side (left in picture) and CO_2 on the bare side (right in picture).

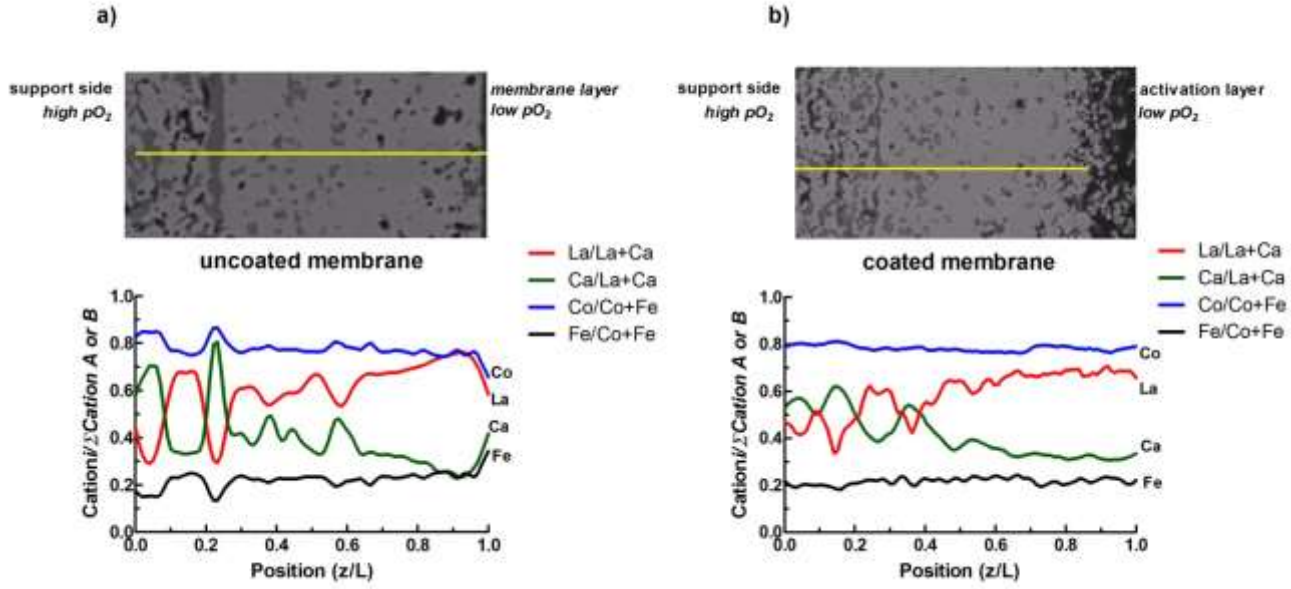

Figure 8. EDS line profile of the cations across the tested membranes: a) uncoated membrane, b) coated membrane.

3.4 Stability testing of LCCF in SO_2-containing atmosphere

SO_2 is among the flue gas contaminants, that the membrane will be exposed to in an oxy-fuel process. The amount of SO_2 in the flue gas depends on the

sulphur content in the feedstock (type of coal or biomass used). The effect of SO_2 on the performance of the membrane should therefore be considered even at very small concentrations. There are few publications in the literature on the impact of SO_2 on the performance of OTM materials, and in most cases reported SO_2 had a poisoning effect on the oxygen permeation [44-47]. The stability of the LCCF membranes towards SO_2 was evaluated over 48 hours at 850 °C exposing them to a gas mixture containing 400 ppm of SO_2. Secondary phases were observed to form on the bare membrane surface. EDS analysis (see Figure 9) confirmed that these comprise mostly O, Ca and S, in accordance with the $CaSO_4$ phase as identified by XRD analysis, **as shown in Fig. 10**. It is noted that the results of the EDS point analyses yield a higher concentration of calcium as compared to sulfur. This results from the fact that the EDS information depth extends into the underlying membrane material, which also contains calcium, whereas sulfur is only abundant in the $CaSO_4$ particles at the surface. S**urface roughness further complicates the accurate assessment of the composition of the formed sulfates.**

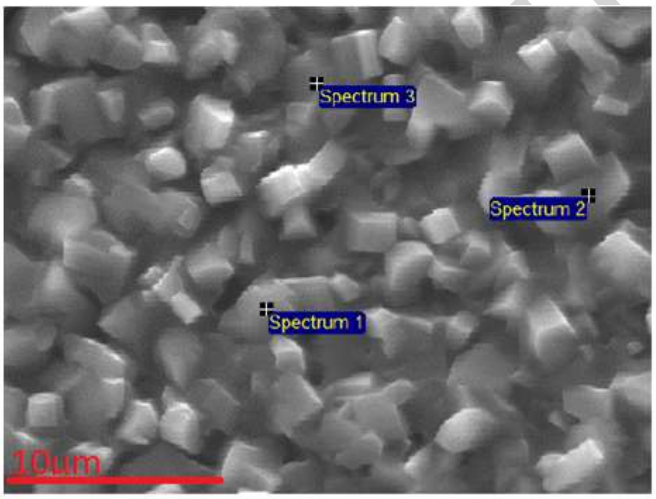

Atom (%)	Spectrum 1	Spectrum 2	Spectrum 3
La	0	0.4	0.3
Ca	15.7	19.4	14.9
Co	0.1	0.4	0.3
Fe	0	0.1	0
O	79.2	70.1	79.9
S	4.9	9.5	4.5

Figure 9. SEM image of surface morphology of the membrane after treatment at 850 °C for 48 h in the presence of 400 ppm SO_2.

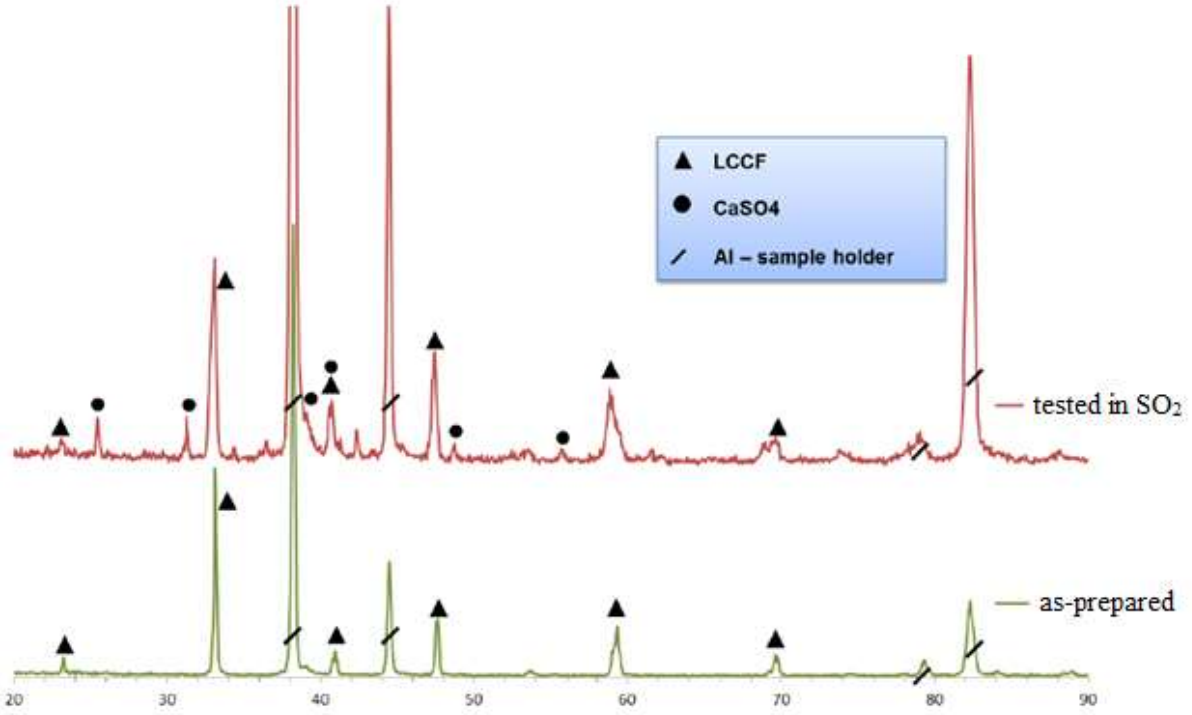

Figure 10. XRD patterns of LCCF a) as prepared, b) tested at 400ppm SO_2/CO_2, 48 h, 850 °C.

Also, SEM images of the cross-section of the membranes (and EDS line profiles, Figure S8 in supporting materials) confirm that sulfates are formed at the surface of the dense membrane layer and at the boundary between the support layer and the membrane layer.

3.5 Kinetic de-mixing of the LCCF membrane

Figures 7 and 8 show an inhomogeneous distribution of cations across the membranes after the oxygen permeation experiments that could indicate a kinetic demixing. **Several authors have reported demixing phenomena across OTMs tested in oxygen chemical potential gradients at high temperature [19, 39, 48-57]. If the mobilities of the cations in the membrane material are different, as a consequence of the Gibbs-Duhem relation, the cations with high diffusion coefficient will be enriched at the high oxygen pressure side. In such condition, the membrane material will consequently demix from an initial homogeneous composition. Demixing process or perhaps more correctly phase separations have also been**

reported for perovskite materials under a uniform oxygen atmosphere [58, 59].

In most cases reported, the observed early stages of a kinetic demixing had no significant effect on the oxygen permeation flux over the periods studied. Buysse *et al.* [48] reported the migration of Sr from the permeate side to the feed side of $Ba_{0.5}Sr_{0.5}Co_{0.8}Fe_{0.2}O_{3-\delta}$ (BSCF) capillary membranes (thickness of 0.4 mm), which were operated for nearly 600 h at 800 to 900 °C. Diethelm *et al.* [49] investigated dense planar and tubular oxygen separation membranes of $La_{0.6}Ca_{0.4}Fe_{0.75}Co_{0.25}O_{3-\delta}$ (thickness of 0.25-1.26 mm) as membrane reactors for partial oxidation (POX) of methane to syngas. SEM and EDS analyses showed that the surface exposed to methane appeared porous, and exhibited a high amount of La, while the surface exposed to air was dense and consisted mostly of Ca and Co with some Fe. Formation of a porous layer enriched in transition metals at the permeate side was observed for $La_{0.4}Ca_{0.6}Fe_{0.75}Co_{0.25}O_{3-\delta}$ membrane exposed to an air/H_2 gradient [19]. Our observations are in line with those of Diethelm *et al.* even though the gradient applied here is only between air or pure oxygen and N_2/CO_2. Wang *et al.* [56] also reported that the secondary phases were found on the surface at the air side of a $La_{0.6}Sr_{0.4}Co_{0.2}Fe_{0.8}O_{3-\delta}$ (LSCF) hollow fibre membrane (thickness of 320 μm), which was tested under 0.21/0.009 oxygen partial pressure (bar) difference at 950°C up to 5000h.

As shown in Figure 11, the most noticeable consequence of the apparent demixing process is near the interface between the support and the dense membrane for both uncoated and coated membranes, where Ca is significantly enriched (the feed side). Tendencies of a depletion can be observed at the permeate side. SEM-EDS results after SO_2 treatment of the LCCF samples at 850 °C for 48 h also revealed that Ca is notably enriched at the boundary between the porous support and the dense membrane layer (see Figure S8 in supporting materials). During the permeation experiment, the Ca-rich phase effectively shifts towards the high pO_2 side of the membrane.

As discussed above, most likely the observed Ca enrichment at the feed side is an effect of a kinetic demixing. A higher diffusivity for Ca in $La_{0.5}Ca_{0.5}Co_{0.8}Fe_{0.2}O_{3-\delta}$ has been reported [60]. Another possible explanation for the observation is that the equilibrium ratio between the two phases is pO_2 dependent, i.e. that the amount of Ca-rich second phase increases with pO_2.

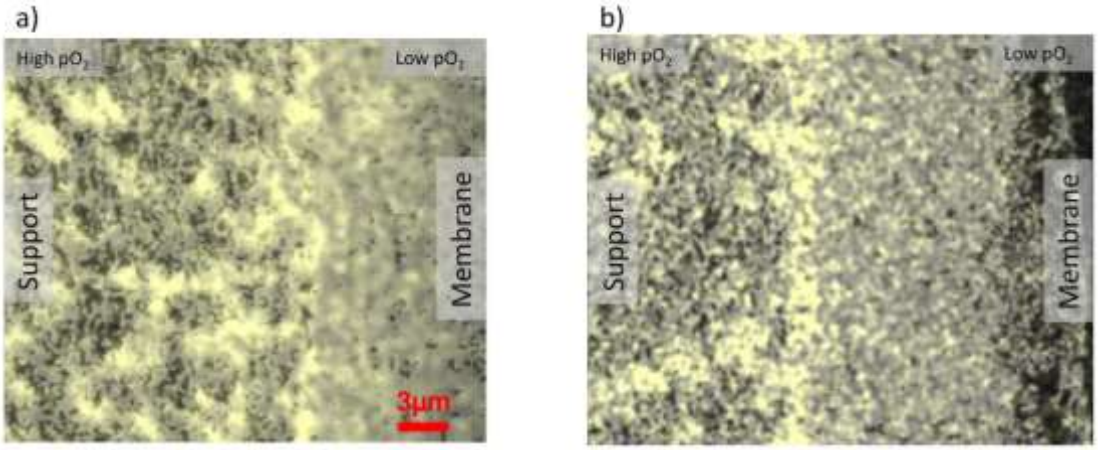

Figure 11. EDS mapping on a polished cross-section of the permeated membrane (Yellow spots reveal the Ca segregation): a) uncoated membrane and b) coated membrane.

During a short two-day stability test, a mild degradation was observed (corresponding to 14%/1000 h, extrapolated). This decrease in oxygen permeation could be due to several reasons. The increased amount of the Ca- and Co-rich phase on the high pO_2 side of the membrane likely formed less conductive phases such as $Ca_2Co_{2-y}Fe_yO_5$ [61, 62], which has a low amount of mobile oxygen vacancies and a non-cubic structure, which may reduce the oxygen reduction reaction rate and charge transfer at the interface between support and dense layer. The other reason could be the chemical contamination caused by glass sealant materials (see Fig. 6). Such contamination results in the decrease of the active surfaces for oxygen exchange reactions on the surface of the membrane [63, 64], and in consequence a decrease in the oxygen permeability as observed in Figure 5.

4. Conclusion

We have reported the oxygen permeation and stability of a supported LCCF membrane (thickness of membrane 25μm) prepared by a tape casting process at different temperatures and at different gas compositions on feed and permeate sides. In summary, **the main conclusions are:**

(1) Coating the surface of the dense layer with a porous LCCF layer (permeate side) improved significantly the oxygen permeation. Also, the oxygen permeation increased with decreasing pO_2 on the permeate side for the coated membrane, while for an uncoated membrane the oxygen permeation went through a maximum and then decreased. **The oxygen flux for the coated membrane reached a maximum of 3.32 Nml cm^{-2} min^{-1} under O_2 at 900°C and 2.06 Nml cm^{-2} min^{-1} under air at 900°C.**

(2) **A secondary phase enriched in Ca was observed on SEM examination of the cross-section of the sintered (as-prepared) membrane. SEM/EDS investigations of membranes tested over two days at 850°C indicated a demixing of the material, by which calcium significantly and cobalt to some degree was enriched on the feed side.**

(3) The results from the SO_2 stability tests showed formation of solid sulfates. Hence, despite that this material is easily processed and shows better stability in CO_2 than that Ba-and Sr-containing analogues, **it is not directly applicable** for use as OTM-material in oxy-fuel process with direct exposure to the flue gas from the boiler**.**

(4) The prepared membranes had a significant amount of a Ca/Co rich second phase, which is undesired as it shifted to the high pO_2 side during operation and reacts with sulphur. The applied 40 % Ca substitution is thus too high and a lower degree of substitution is recommended for further development.

Acknowledgements

The authors would like to acknowledge the financial contribution provided by GREEN-CC project (Grant Agreement Number: 608524). The authors also would like to thank Dr. S. Ovtar at Department of Energy Conversion and Storage, Technical University of Denmark for her kind help in the treatment of the XRD data. The help of Henrik Paulsen in polishing the samples for microscopy and Marianne Nielsen for preparing the final tape is greatly appreciated.

References

[1] B.Y. Li, Y.H. Duan, D. Luebke, B. Morreale, Advances in CO2 capture technology: A patent review, Appl. Energy, 102 (2013) 1439-1447.
[2] J.D. Figueroa, T. Fout, S. Plasynski, H. McIlvried, R.D. Srivastava, Advances in CO2 capture technology—The U.S. Department of Energy's Carbon Sequestration Program, International Journal of Greenhouse Gas Control, 2 (2008) 9-20.
[3] X. Dong, W. Jin, Mixed conducting ceramic membranes for high efficiency power generation with CO2 capture, Current Opinion in Chemical Engineering, 1 (2012) 163-170.
[4] M.A. Habib, H.M. Badr, S.F. Ahmed, R. Ben-Mansour, K. Mezghani, S. Imashuku, G.J. la O, Y. Shao-Horn, N.D. Mancini, A. Mitsos, P. Kirchen, A.F. Ghoneim, A review of recent developments in carbon capture utilizing oxy-fuel combustion in conventional and ion transport membrane systems, International Journal of Energy Research, 35 (2011) 741-764.
[5] L. Zheng, Oxy-fuel combustion for power generation and carbon dioxide (CO2) capture, Elsevier, 2011.
[6] S.M. Hashim, A.R. Mohamed, S. Bhatia, Current status of ceramic-based membranes for oxygen separation from air, Adv. Colloid Interface Sci., 160 (2010) 88-100.
[7] S. Smart, C. Lin, L. Ding, K. Thambimuthu, J.D. Da Costa, Ceramic membranes for gas processing in coal gasification, Energy & Environmental Science, 3 (2010) 268-278.
[8] Y.Y. Wei, W.S. Yang, J. Caro, H.H. Wang, Dense ceramic oxygen permeable membranes and catalytic membrane reactors, Chemical Engineering Journal, 220 (2013) 185-203.
[9] M. Puig-Arnavat, S. Soprani, M. Søgaard, K. Engelbrecht, J. Ahrenfeldt, U.B. Henriksen, P.V. Hendriksen, Integration of mixed conducting membranes in an oxygen–steam biomass gasification process, Rsc Advances, 3 (2013) 20843-20854.
[10] Y. Wei, W. Yang, J. Caro, H. Wang, Dense ceramic oxygen permeable membranes and catalytic membrane reactors, Chemical Engineering Journal, 220 (2013) 185-203.
[11] P.M. Geffroy, J. Fouletier, N. Richet, T. Chartier, Rational selection of MIEC materials in energy production processes, Chemical Engineering Science, 87 (2013) 408-433.
[12] J. Sunarso, S. Baumann, J.M. Serra, W.A. Meulenberg, S. Liu, Y.S. Lin, J.C.D. da Costa, Mixed ionic-electronic conducting (MIEC) ceramic-based membranes for oxygen separation, Journal of Membrane Science, 320 (2008) 13-41.
[13] K. Efimov, T. Klande, N. Juditzki, A. Feldhoff, Ca-containing CO2-tolerant perovskite materials for oxygen separation, Journal of Membrane Science, 389 (2012) 205-215.
[14] B.V. L'vov, Mechanism and kinetics of thermal decomposition of carbonates, Thermochimica acta, 386 (2002) 1-16.

[15] Y. Teraoka, T. Nobunaga, N. Yamazoe, Effect of Cation Substitution on the Oxygen Semipermeability of Perovskite-type Oxides, Chemistry Letters, 17 (1988) 503-506.
[16] K. Watanabe, M. Yuasa, T. Kida, K. Shimanoe, Y. Teraoka, N. Yamazoe, Preparation of oxygen evolution layer/La0.6Ca0.4CoO3 dense membrane/porous support asymmetric structure for high-performance oxygen permeation, Solid State Ionics, 179 (2008) 1377-1381.
[17] K. Watanabe, M. Yuasa, T. Kida, K. Shimanoe, Y. Teraoka, N. Yamazoe, Dense/Porous Asymmetric-Structured Oxygen Permeable Membranes Based on La0.6Ca0.4CoO3 Perovskite-Type Oxide, Chemistry of Materials, 20 (2008) 6965-6973.
[18] J.W. Stevenson, T.R. Armstrong, R.D. Carneim, L.R. Pederson, W.J. Weber, Electrochemical properties of mixed conducting perovskites La1-xMxCo1-yFeyO3-δ (M = Sr, Ba, Ca), Journal of the Electrochemical Society, 143 (1996) 2722-2729.
[19] S. Diethelm, J. Van herle, P.H. Middleton, D. Favrat, Oxygen permeation and stability of La0.4Ca0.6Fe1−xCoxO3−δ (x = 0, 0.25, 0.5) membranes, Journal of Power Sources, 118 (2003) 270-275.
[20] P. Gordes, N. Christiansen, E. Jensen, J. Villadsen, Synthesis of perovskite-type compounds by drip pyrolysis, Journal of materials science, 30 (1995) 1053-1058.
[21] S. Cheng, M. Sogaard, L. Han, W. Zhang, M. Chen, A. Kaiser, P.V. Hendriksen, A novel CO2- and SO2-tolerant dual phase composite membrane for oxygen separation, Chemical Communications, 51 (2015) 7140-7143.
[22] A.J. Samson, M. Søgaard, P. Vang Hendriksen, (Ce,Gd)O2−δ-based dual phase membranes for oxygen separation, Journal of Membrane Science, 470 (2014) 178-188.
[23] K.A. Nielsen, M. Solvang, S.B.L. Nielsen, A.R. Dinesen, D. Beeaff, P.H. Larsen, Glass composite seals for SOFC application, J. Eur. Ceram. Soc., 27 (2007) 1817-1822.
[24] A.S. Harvey, F.J. Litterst, Z. Yang, J.L.M. Rupp, A. Infortuna, L.J. Gauckler, Oxidation states of Co and Fe in Ba1-xSrxCo1-yFeyO3-delta (x, y=0.2-0.8) and oxygen desorption in the temperature range 300-1273 K, Physical Chemistry Chemical Physics, 11 (2009) 3090-3098.
[25] E. Bucher, A. Egger, G.B. Caraman, W. Sitte, Stability of the SOFC cathode material (Ba,Sr)(Co,Fe)O(3-delta) in CO(2)-containing atmospheres, Journal of the Electrochemical Society, 155 (2008) B1218-B1224.
[26] V. Esposito, M. Sogaard, P.V. Hendriksen, Chemical stability of La0.6Sr0.4CoO3-delta in oxygen permeation applications under exposure to N-2 and CO2, Solid State Ionics, 227 (2012) 46-56.
[27] Z. Yang, J. Martynczuk, K. Efimov, A.S. Harvey, A. Infortuna, P. Kocher, L.J. Gauckler, Oxygen-Vacancy-Related Structural Phase Transition of Ba0.8Sr0.2Co0.8Fe0.2O3-delta, Chemistry of Materials, 23 (2011) 3169-3175.
[28] I. Galan, F.P. Glasser, C. Andrade, Calcium carbonate decomposition, Journal of Thermal Analysis and Calorimetry, 111 (2013) 1197-1202.
[29] S. Pathak, J. Kuebler, A. Payzant, N. Orlovskaya, Mechanical behavior and electrical conductivity of La< sub> 1− x</sub> Ca< sub> x</sub> CoO< sub> 3</sub>(< i> x</i>= 0, 0.2, 0.4, 0.55) perovskites, Journal of Power Sources, 195 (2010) 3612-3620.
[30] S. Baumann, J.M. Serra, M.P. Lobera, S. Escolastico, F. Schulze-Kueppers, W.A. Meulenberg, Ultrahigh oxygen permeation flux through supported Ba0.5Sr0.5Co0.8Fe0.2O3-delta membranes, Journal of Membrane Science, 377 (2011) 198-205.
[31] J. Gurauskis, O.F. Lohne, K. Wiik, La0.2Sr0.8Fe0.8Ta0.2O3 (-) (delta) based thin film membranes with surface modification for oxygen production, Solid State Ionics, 225 (2012) 703-706.
[32] V.V. Kharton, A. Kovalevsky, A.A. Yaremchenko, F.M. Figueiredo, E.N. Naumovich, A.L. Shaulo, F.M.B. Marques, Surface modification of La0.3Sr0.7C0O3-delta ceramic membranes, Journal of Membrane Science, 195 (2002) 277-287.
[33] A. Kovalevsky, C. Buysse, F. Snijkers, A. Buekenhoudt, J. Luyten, J. Kretzschmar, S. Lenaerts, Oxygen exchange-limited transport and surface activation of Ba0.5Sr0.5Co0.8Fe0.2O3-delta capillary membranes, Journal of Membrane Science, 368 (2011) 223-232.

[34] J.M. Serra, J. Garcia-Fayos, S. Baumann, F. Schulze-Kueppers, W.A. Meulenberg, Oxygen permeation through tape-cast asymmetric all-La0.6Sr0.4Co0.2Fe0.8O3 (-) (delta) membranes, Journal of Membrane Science, 447 (2013) 297-305.
[35] P.-M. Geffroy, A. Vivet, J. Fouletier, N. Richet, P. Del Gallo, T. Chartier, Influence of Oxygen Surface Exchanges on OxygenSemi-Permeation through La (1− x) SrxFe (1− y) GayO3− δDense Membrane, Journal of the Electrochemical Society, 158 (2011) B971-B979.
[36] M. Søgaard, P. Vang Hendriksen, M. Mogensen, Oxygen nonstoichiometry and transport properties of strontium substituted lanthanum ferrite, Journal of Solid State Chemistry, 180 (2007) 1489-1503.
[37] S. Li, W. Jin, P. Huang, N. Xu, J. Shi, Y. Lin, M.Z.-C. Hu, E.A. Payzant, Comparison of oxygen permeability and stability of perovskite type La0. 2A0. 8Co0. 2Fe0. 8O3-δ (A= Sr, Ba, Ca) Membranes, Industrial & engineering chemistry research, 38 (1999) 2963-2972.
[38] S. Cheng, H. Huang, S. Ovtar, S.B. Simonsen, M. Chen, W. Zhang, M. Søgaard, A. Kaiser, P.V. Hendriksen, C. Chen, High-Performance Microchanneled Asymmetric Gd0. 1Ce0. 9O1. 95− δ–La0. 6Sr0. 4FeO3− δ-Based Membranes for Oxygen Separation, ACS applied materials & interfaces, 8 (2016) 4548-4560.
[39] H.L. Lein, K. Wiik, T. Grande, Kinetic demixing and decomposition of oxygen permeable membranes, Solid State Ionics, 177 (2006) 1587-1590.
[40] P. Zeng, R. Ran, Z. Chen, H. Gu, Z. Shao, S. Liu, Novel mixed conducting SrSc0.05Co0.95O3-δ ceramic membrane for oxygen separation, AIChE Journal, 53 (2007) 3116-3124.
[41] B.T. Dalslet, M. Søgaard, P.V. Hendriksen, Determination of oxygen transport properties from flux and driving force measurements, Journal of the Electrochemical Society, 154 (2007) B1276-B1287.
[42] P.M. Geffroy, A. Vivet, J. Fouletier, N. Richet, P. Del Gallo, T. Chartier, Influence of Oxygen Surface Exchanges on OxygenSemi-Permeation through La(1−x)SrxFe(1−y)GayO3−δDense Membrane, Journal of the Electrochemical Society, 158 (2011) B971-B979.
[43] O. Paulsen, Rigid bonded glass ceramic seals for high temperature membrane reactors and solid oxide fuel cells, (2009).
[44] S. Engels, T. Markus, M. Modigell, L. Singheiser, Oxygen permeation and stability investigations on MIEC membrane materials under operating conditions for power plant processes, Journal of Membrane Science, 370 (2011) 58-69.
[45] J. Gao, L. Li, Z. Yin, J. Zhang, S. Lu, X. Tan, Poisoning effect of SO 2 on the oxygen permeation behavior of La 0.6 Sr 0.4 Co 0.2 Fe 0.8 O 3− δ perovskite hollow fiber membranes, Journal of Membrane Science, 455 (2014) 341-348.
[46] Y. Wei, Q. Liao, J. Xue, Z. Li, H. Wang, Influence of SO 2 on the phase structure, oxygen permeation and microstructure of K 2 NiF 4-type hollow fiber membranes, Chemical Engineering Journal, 217 (2013) 34-40.
[47] Y. Wei, O. Ravkina, T. Klande, H. Wang, A. Feldhoff, Effect of CO 2 and SO 2 on oxygen permeation and microstructure of (Pr 0.9 La 0.1) 2 (Ni 0.74 Cu 0.21 Ga 0.05) O 4+ δ membranes, Journal of Membrane Science, 429 (2013) 147-154.
[48] C. Buysse, A. Kovalevsky, F. Snijkers, A. Buekenhoudt, S. Mullens, J. Luyten, J. Kretzschmar, S. Lenaerts, Development, performance and stability of sulfur-free, macrovoid-free BSCF capillaries for high temperature oxygen separation from air, Journal of Membrane Science, 372 (2011) 239-248.
[49] S. Diethelm, J. Sfeir, F. Clemens, J. Van Herle, D. Favrat, Planar and tubular perovskite-type membrane reactors for the partial oxidation of methane to syngas, Journal of Solid State Electrochemistry, 8 (2004) 611-617.
[50] F. Iguchi, N. Sata, H. Yugami, H. Takamura, Oxygen permeation properties and the stability of La0.6Sr0.4Fe0.8Co0.2O3 studied by Raman spectroscopy, Solid State Ionics, 177 (2006) 2281-2284.
[51] J.I. Jung, D.D. Edwards, Kinetic demixing/decomposition of Ba0.5Sr0.5CoxFe1-xO3-delta (x=0.2 and 0.8), J. Eur. Ceram. Soc., 32 (2012) 3733-3743.

[52] D. Schlehuber, E. Wessel, L. Singheiser, T. Markus, Long-term operation of a La0.58Sr0.4Co0.2Fe0.8O3-delta-membrane for oxygen separation, Journal of Membrane Science, 351 (2010) 16-20.
[53] X. Tan, Z. Pang, K. Li, Oxygen production using La0.6Sr0.4Co0.2Fe0.8O3-alpha (LSCF) perovskite hollow fibre membrane modules, Journal of Membrane Science, 310 (2008) 550-556.
[54] R.H.E. van Doorn, H.J.M. Bouwmeester, A.J. Burggraaf, Kinetic decomposition of La0.3Sr0.7CoO3-delta perovskite membranes during oxygen permeation, Solid State Ionics, 111 (1998) 263-272.
[55] J.F. Vente, S. McIntosh, W.G. Haije, H.J.M. Bouwmeester, Properties and performance of BaxSr1-xCo0.8Fe0.2O3-delta materials for oxygen transport membranes, Journal of Solid State Electrochemistry, 10 (2006) 581-588.
[56] B. Wang, B. Zydorczak, D. Poulidi, I.S. Metcalfe, K. Li, A further investigation of the kinetic demixing/decomposition of La0.6Sr0.4Co0.2Fe0.8O3-delta oxygen separation membranes, Journal of Membrane Science, 369 (2011) 526-535.
[57] B. Wang, B. Zydorczak, Z.-T. Wu, K. Li, Stabilities of La0.6Sr0.4Co0.2Fe0.8O3-delta oxygen separation membranes-Effects of kinetic demixing/decomposition and impurity segregation, Journal of Membrane Science, 344 (2009) 101-106.
[58] D. Oh, D. Gostovic, E.D. Wachsman, Mechanism of La 0.6 Sr 0.4 Co 0.2 Fe 0.8 O 3 cathode degradation, Journal of Materials Research, 27 (2012) 1992-1999.
[59] X. Wang, T. Miyazaki, K. Yashiro, S. Hashimoto, T. Kawada, The Origin of Instability of Lanthanum Strontium Cobalt Ferrite (La–Sr–Co–Fe–O; LSCF) under Oxygen Potential Gradient, ECS Transactions, 75 (2017) 1-9.
[60] J. Hjelm, P. Hjalmarsson, R. Knibbe, A. Hauch, C.R. Graves, W.-R. Kiebach, D. Curran, H.L. Frandsen, T. Ramos, S.L. Ebbehøj, Durable and Robust Solid Oxide Fuel Cells, in, energinet. dk, 2012.
[61] A.L. Shaula, Y.V. Pivak, J.C. Waerenborgh, P. Gaczyñski, A.A. Yaremchenko, V.V. Kharton, Ionic conductivity of brownmillerite-type calcium ferrite under oxidizing conditions, Solid State Ionics, 177 (2006) 2923-2930.
[62] S. Yu, S. He, H. Chen, L. Guo, Effect of calcination temperature on oxidation state of cobalt in calcium cobaltite and relevant performance as intermediate-temperature solid oxide fuel cell cathodes, Journal of Power Sources, 280 (2015) 581-587.
[63] Y. Chen, B. Qian, Y. Hao, S. Liu, M.O. Tade, Z. Shao, Influence of sealing materials on the oxygen permeation fluxes of some typical oxygen ion conducting ceramic membranes, Journal of Membrane Science, 470 (2014) 102-111.
[64] A. Vivet, P.-M. Geffroy, V. Coudert, J. Fouletier, N. Richet, T. Chartier, Influence of glass and gold sealants materials on oxygen permeation performances in La 0.8 Sr 0.2 Fe 0.7 Ga 0.3 O 3− δ perovskite membranes, Journal of Membrane Science, 366 (2011) 132-138.

Highlights:

- A 25µm asymmetric LCCF membrane was prepared by tape casting.
- Secondary phases were formed during the sintering of the membrane.
- Modification of the membrane surface improved oxygen permeation flux.
- Post-test examinations showed evidence of a kinetic de-mixing.
- **Sulfate formed on the membrane surface after exposure to SO_2.**